University of Pennsylvania
ScholarlyCommons

Departmental Papers (CBE)

Department of Chemical & Biomolecular Engineering

11-1-2005

Structure and Thermal Stability of Ceria Films Supported on YSZ(100) and α-Al_2O_3(0001)

Olga Costa-Nunes
University of Pennsylvania

Robert M. Ferrizz
Sandia National Laboratories

Raymond J. Gorte
University of Pennsylvania, gorte@seas.upenn.edu

John M. Vohs
University of Pennsylvania, vohs@seas.upenn.edu

Postprint version. Published in *Surface Science*, Volume 592, Issues 1-3, November 1, 2005, pages 8-17.
Publisher URL: http://dx.doi.org/10.1016/j.susc.2005.06.029

This paper is posted at ScholarlyCommons. http://repository.upenn.edu/cbe_papers/62
For more information, please contact repository@pobox.upenn.edu.

Structure and Thermal Stability of Ceria Films Supported on YSZ(100) and α-Al_2O_3(0001)

Abstract

The morphology and reducibility of vapor-deposited ceria films supported on yttria-stabilized zirconia (100) (YSZ(100)) and α-Al_2O_3(0001) single crystals were studied using X-ray photoelectron spectroscopy (XPS) and atomic force microscopy (AFM). The results of this study show that the gas environment has a significant effect on the structure of the ceria films on both substrates. CeO_2 films on α-Al_2O_3(0001) were found to be stable in a reducing environment at temperatures up to 1000K, but underwent agglomeration and reaction with the support to form $CeAlO_3$ upon annealing at 1273 K in air. Heating CeO_2/YSZ(100) in air at 1273 K caused the ceria thin film to agglomerate into bar-shaped features which were re-dispersed by subsequent annealing in vacuum. Interactions at the CeO_2-YSZ interface were also found to dramatically enhance the reducibility of ceria films supported on YSZ(100).

Keywords

Ceria, Zirconia, Al_2O_3, X-ray photoelectron spectroscopy, Atomic force microscopy

Comments

Postprint version. Published in *Surface Science*, Volume 592, Issues 1-3, November 1, 2005, pages 8-17.
Publisher URL: http://dx.doi.org/10.1016/j.susc.2005.06.029

This journal article is available at ScholarlyCommons: http://repository.upenn.edu/cbe_papers/62

Structure and Thermal Stability of Ceria Films Supported on YSZ(100) and α-Al_2O_3(0001)

O. Costa-Nunes [a], R.M. Ferrizz [b], R.J. Gorte [a], J.M. Vohs [a,*]

[a] *Department of Chemical and Biomolecular Engineering, University of Pennsylvania, Philadelphia, PA 19104, USA*
[b] *Sandia National Laboratories, New Mexico, Albuquerque, NM 87185 , USA*

Abstract

The morphology and reducibility of vapor-deposited ceria films supported on yttria-stabilized zirconia (100) (YSZ(100)) and α-Al_2O_3(0001) single crystals were studied using X-ray photoelectron spectroscopy (XPS) and atomic force microscopy (AFM). The results of this study show that the gas environment has a significant effect on the structure of the ceria films on both substrates. CeO_2 films on α-Al_2O_3(0001) were found to be stable in a reducing environment at temperatures up to 1000K, but underwent agglomeration and reaction with the support to form $CeAlO_3$ upon annealing at 1273 K in air. Heating CeO_2/YSZ(100) in air at 1273 K caused the ceria thin film to agglomerate into bar-shaped features which were re-dispersed by subsequent annealing in vacuum. Interactions at the CeO_2-YSZ interface were also found to dramatically enhance the reducibility of ceria films supported on YSZ(100).

Keywords: Ceria, Zirconia, Al_2O_3; X-ray photoelectron spectroscopy; Atomic force microscopy.

**corresponding author*

1. Introduction

Ceria is an important component in automotive emissions-control catalysis where its ability to store and release oxygen is used to compensate for changes in the partial pressure of oxygen and maintain the stoichiometric oxygen-to-fuel ratio which is required for optimal catalyst performance [1-8]. This so-called oxygen storage capacity (OSC) of ceria relies on the ability of the cerium cations to cycle between +4 and +3 oxidation states under oxidizing and reducing conditions. These redox properties of ceria are known to be influenced by interactions with other metal oxides such as zirconia [1-3,9]. Indeed, ceria supported on zirconia and mixed oxides of ceria and zirconia have higher oxygen storage capacity than ceria alone [3,9-12]. The interest in interactions between ceria and zirconia also extends to solid oxide fuel cells where ceria is commonly used as an anode oxidation catalyst which is in contact with the oxygen, ion-conducting electrolyte, yttria-stabilized zirconia (YSZ) [13-18]. Interactions between ceria and alumina are also important in automotive catalysts where it has been shown that ceria can help stabilize the surface area of the γ-Al_2O_3 support [19,20,21]. Several studies indicate that this stabilization results from the formation of cerium aluminate ($CeAlO_3$) and that the extent of the stabilization depends on a variety of factors including ceria dispersion, temperature, and gas environment [19-23].

Due to the importance of ceria in these applications, the reactivity of model catalysts consisting of ceria films on single crystal YSZ and α-Al_2O_3 supports has been the subject of several previous studies [9,20,21,24-32]. When YSZ(100) and YSZ(110) are used as the substrate, vapor deposited ceria films have been shown to grow epitaxially. In contrast, when the support is α-Al_2O_3(0001) polycrystalline films are produced [9,28,30]. These studies also suggest that interactions at the ceria-substrate interface can influence both the reducibility and

reactivity of the ceria. For example, our previous TPD results have indicated that polycrystalline CeO_2 films supported on α-Al_2O_3(0001) are stable in vacuum to temperatures in excess of 1000 K while, epitaxial CeO_2 films supported on YSZ(100) partially reduce upon heating to only 750 K [29]. It should be noted, however, that this conclusion was based on indirect evidence and XPS results where not completely consistent with this conclusion and indicated that CeO_2 films on both YSZ(100) and α-Al_2O_3(0001) were partially reduced upon heating to 750 K in vacuum with the extent of reduction being higher for CeO_2/YSZ(100). It was speculated that this discrepancy between the XPS and TPD results was due to prolonged exposure of the samples used in the XPS experiments to air, resulting in carbon contamination which may have acted as a reductant.

In a recent letter we have reported the initial results of an atomic force microcopy (AFM) study that showed that the structure of ceria films on YSZ(100) is dependent on both gas environment and temperature [33]. Annealing a 4 nm thick, epitaxial CeO_2 film on YSZ(100) in air at 1273 K resulted in agglomeration of the ceria into well-defined, bar-shaped islands. Subsequent annealing in reducing atmospheres caused the ceria islands to partially redistribute over the surface of the YSZ(100) support. In the work reported here we provide a more detailed description of our studies of the effect of temperature and gas environments on the structure and stability of ceria films on YSZ(100) and have expanded these studies to include ceria films supported on α-Al_2O_3(0001). XPS results obtained using more carefully controlled conditions than in our previous study are also presented and provide a definitive answer to the question of the thermal stability of CeO_2 films on YSZ(100) and α-Al_2O_3(0001) in vacuum.

2. Experimental Methods

Ceria films, 4 nm in thickness, were grown on YSZ(100) and α-Al_2O_3(0001) substrates (MTI Corporation) by initially depositing a layer of cerium metal using an evaporative cerium source followed by annealing in oxygen or air. A quartz crystal film thickness monitor was used to determine the film thickness during growth. Two separate vacuum chambers were used for ceria film deposition. One chamber consisted of a multi-technique, ultra-high vacuum (UHV) surface analysis system with a base pressure of $1x10^{-10}$ Torr that was equipped with an evaporative Ce source, a film thickness monitor (Maxtek), ion sputter gun (Physical Electronics), X-ray source (VGMicrotech), and hemispherical electron energy analyzer (Leybold–Heraeus). This chamber was also equipped with a load-lock for rapid introduction of samples into the system. The other chamber was used exclusively for film deposition and was equipped with an evaporative cerium source and a film thickness monitor (Maxtek) and had a base pressure of $1x10^{-8}$ Torr.

In the UHV system, the YSZ(100) and α-Al_2O_3(0001) substrates were cleaned using cycles of sputtering with 2 kV Ar^+ ions for 30 min followed by annealing at 750 K for 60 min, until the surface was free of impurities as determined by XPS. For both substrates cerium metal was deposited using the evaporative cerium source with the sample held at room temperature. The sample was then annealed in $1x10^{-7}$ Torr of O_2 at 450 K for 15 min. This oxidation treatment produced fully oxidized CeO_2 films as judged by XPS. One of the CeO_2/YSZ(100) samples was prepared in the dedicated film growth chamber. For this sample, a previously cleaned YSZ(100) support was initially annealed at 973 K in order to desorb water and other adsorbed species. A cerium film was then deposited using the evaporative cerium source with

the sample held at room temperature. This sample was then removed from vacuum and annealed in air at 773 K in order to insure that the CeO_2 layer was fully oxidized.

The binding energy scale in the XPS spectra was referenced to the O(1s) photoemission peak which was set at 529.6 eV. Atomic force microscopy (AFM) was used to characterize the morphology of the ceria films as a function of pretreatment conditions. All AFM experiments were performed in air using a Digital Instruments Nanoscope operated in the tapping mode.

3. Results

3.1. XPS

3.1.1. CeO_2/YSZ(100)

Ce(3d) XP spectra obtained from a CeO_2/YSZ(100) sample that was prepared in the UHV system as a function of sample pre-treatment conditions are displayed in Figure 1. As described in the experimental section, the 4 nm ceria film was grown by depositing cerium metal followed by annealing in 10^{-7} Torr of O_2 at 450 K for 15 min. Spectrum A in the figure was obtained after heating the as-grown ceria film to 600 K. This spectrum is consistent with that reported in the literature for Ce^{+4} [34-39]. The peaks corresponding to the $3d_{3/2}$ and $3d_{5/2}$ states are labeled u and v, respectively. The u´´´/v´´´ doublet is due to the primary photoemission process, while the u/v and u´´/v´´ doublets are shakedown features resulting from transfer of one or two electrons from the filled O(2p) orbital to an empty Ce(4f) orbital during photoemission [34-39].

Heating the CeO_2/YSZ(100) sample to 750 K (spectrum B) did not produce any significant changes in Ce(3d) spectrum, which was still indicative of Ce^{+4}. Heating to 825 K, however (spectrum C), resulted in the appearance of two new sets of doublets which are labeled

u´/v´, u_0/v_0 in the figure. These peaks are in positions consistent with those reported in the literature for Ce^{3+} cations [34-39]. The u´/v´ doublet is due to the primary photoemission process while the u_0/v_0 doublet is a shakedown feature. The appearance of these peaks demonstrates that partial reduction of the ceria layer occurs upon heating to 825 K in vacuum. Heating the sample to 900 K caused more substantial reduction of the ceria film. The XP spectrum obtained after heating to this temperature (spectrum D) is dominated by the peaks due to Ce^{3+}. These XPS results are consistent with those reported previously by Ferrizz et al. [29] and show that CeO_2 films supported on YSZ(100) undergo reduction to Ce_2O_3 upon heating to 900 K in vacuum.

Ce(3d) XP spectra obtained from a CeO_2/YSZ(100) sample that was annealed in air, rather than vacuum, have been reported previously [33]. In this earlier study it was found that the Ce(3d) spectrum of a freshly prepared CeO_2/YSZ(100) sample that was annealed in air at 773 K for 12 hrs was nearly identical to that obtained from the ceria film annealed in 10^{-7} Torr of O_2 at 450 K for 15 min shown in Figure 1. As shown in Table 1, which lists the Ce(3d)/Zr(3d) peak area ratio for this sample as a function of pretreatment conditions, annealing this sample in air at 1273 K for 12 hrs, however, produced a decrease in the Ce(3d)/Zr(3d) peak area ratio from 20.6 to 2.3. This result suggests a change in the morphology of the ceria film upon heating to 1273 K in air. The AFM results presented below confirm this and show that the ceria film agglomerates into particles upon annealing in air at high temperatures.

Heating the CeO_2/YSZ(100) sample that had previously been annealed in air at 1273 K to 873 K in vacuum for 2 hrs caused complete reduction of the CeO_2 film to Ce_2O_3 [33] but had little effect on the Ce(3d)/Zr(3d) peak area ratio(Table 1). This result is consistent with the data shown in Figure 1 for the sample that was annealed in 10^{-7} Torr of O_2 and again demonstrates the

reduction of the YSZ-supported ceria films upon heating to temperatures in excess of 873 K in vacuum. Further annealing of this sample in vacuum at 973 K for 4 hours resulted in an increase in the Ce(3d)/Zr(3d) peak area ratio from 2.2 to 4.1. This observation suggests further changes in the morphology the ceria layer. The AFM results presented below demonstrate that re-dispersion of the ceria layer occurs upon heating in vacuum.

3.1.2. $CeO_2/\alpha\text{-}Al_2O_3(0001)$

XPS was also used to characterize ceria films supported on $\alpha\text{-}Al_2O_3(0001)$. Figure 2 shows Ce(3d) XP spectra as a function of annealing temperature obtained from a $CeO_2/\alpha\text{-}Al_2O_3(0001)$ sample that was prepared in the UHV chamber. Spectrum A in this figure corresponds to a freshly prepared $CeO_2/\alpha\text{-}Al_2O_3(0001)$ sample that had been briefly heated to 550 K. This spectrum contains the u´´´/v´´´, u´´/v´´, and u/v doublets for Ce^{+4} indicating a fully oxidized ceria layer. In contrast to the CeO_2/YSZ(100) sample, heating the $CeO_2/\alpha\text{-}Al_2O_3(0001)$ sample to 900 K in vacuum did not result in the reduction of the ceria layer and the spectrum (D) obtained after heating to this temperature was still indicative of Ce^{+4}. Furthermore, even after heating the $CeO_2/\alpha\text{-}Al_2O_3(0001)$ sample to 1000 K in vacuum, the XP spectrum (E) still showed primarily Ce^{+4}. Heating in vacuum also did not cause a change in the Ce(3d)/Al(2p) peak area ratio for this sample. As noted in the introduction, in a previous study it was observed that some reduction of a CeO_2 film on $\alpha\text{-}Al_2O_3(0001)$ occurred upon heating in vacuum to only 750 K . It was thought, however, that this result may have been due to surface carbon contamination. The results presented here, therefore, provide a more definitive answer to the question of the reducibility of CeO_2 films on $\alpha\text{-}Al_2O_3(0001)$ upon heating in vacuum and show that $CeO_2/\alpha\text{-}Al_2O_3(0001)$ is stable to temperatures in excess of 1000 K.

The effect of annealing a $CeO_2/\alpha\text{-}Al_2O_3(0001)$ sample in air was also studied. Figure 3 displays XP spectra obtained from a $CeO_2/\alpha\text{-}Al_2O_3(0001)$ sample annealed in air at temperatures up to 1273 K. Spectrum A in this figure corresponds to a freshly prepared sample that was annealed in air at 773 K. This spectrum is indicative of Ce^{+4} demonstrating that that the ceria film is fully oxidized. Annealing this sample in air at 973 K for 12 hrs produced a large decrease in the intensity of 3d peaks from Ce^{+4} as shown by spectrum B in Figure 3. Table 2 lists the ratio of the area of the Ce(3d) peak to that of the Al(2p) peak from the substrate for the samples in Figure 4. Note that the Ce(3d)/Al(2p) ratio decreased from 97 to 7 upon increasing the annealing temperature from 773 to 1273 K. As was also the case for the CeO_2/YSZ(100) sample, this result indicates a change in the morphology of the ceria film.

Annealing the $CeO_2/\alpha\text{-}Al_2O_3(0001)$ sample in air to higher temperatures resulted in reduction of a significant fraction of the Ce cations from +4 to +3 and relatively small changes in the Ce(3d)/Al(2p) ratio. Spectrum C was obtained after annealing in air at 1273 K for 12 hrs and contains peaks for both oxidation states. Furthermore, heating this sample in vacuum to 873 K resulted in further reduction of the ceria (spectrum D). The most likely explanation for these results is that under oxidizing conditions ceria and alumina react at temperatures near 1073 K to form $CeAlO_3$. Note that the results in Figure 3 show that this reaction does not occur when a $CeO_2/\alpha\text{-}Al_2O_3(0001)$ sample is heated to 1000 K in vacuum. Thus, the oxidizing environment plays a role in promoting the formation of the cerium aluminate.

3.2 – AFM

AFM was used to characterize the structure of the ceria films on the YSZ(100) and $\alpha\text{-}Al_2O_3(0001)$ substrates as a function of the pretreatment conditions. Figure 4 displays 1 μm x 1

μm AFM images of the CeO_2/YSZ(100) sample. Panel A in this figure corresponds to a freshly prepared CeO_2/YSZ(100) sample that was annealed in air at 773 K. The image shows a fairly smooth surface, with a rms roughness of 0.7 nm which is similar to that of the clean YSZ(100) surface prior to ceria deposition and indicates that the ceria film completely covers the surface. This result is consistent with previous studies that show that vapor-deposited ceria films grow epitaxially on YSZ(100) [9,28,30].

The AFM image of the CeO_2/YSZ(100) sample after annealing at 1273 K in air is displayed in Figure 4-B. This image shows that the heat treatment caused the ceria to agglomerate into well-defined bar-shaped structures that are aligned with several distinct crystallographic directions suggesting that the bars maintain an epitaxial arrangement with the YSZ substrate. Agglomeration of the ceria film is consistent with the decrease in the Ce(3d)/Zr(3d) peak area ratio in the XPS spectra upon heating a CeO_2/YSZ(100) in air (Table 1). Analysis of the AFM image reveals that the agglomerates have a relatively uniform height (~18 nm) and width. We have previously shown that the volume occupied by the bar-shaped features roughly corresponds to the amount of ceria deposited on the substrate and that these features can be dissolved in nitric acid [33]. Based on these observations it was concluded that the bar-shaped features are composed of ceria rather than a mixed oxide of ceria and zirconia.

Heating the sample containing ceria agglomerates in vacuum at 973 K caused partial re-dispersion of the ceria, as shown in Figure 4-C. This AFM image shows that the morphology of the surface features has dramatically changed, with the bar-shaped agglomerates becoming broader and much more irregular in shape. This is consistent with the XPS data presented in Table 1 which showed an increase in the Ce(3d)/Zr(3d) ratio after heating the sample in vacuum.

Figure 5 displays 1 μm x 1μm AFM images of the $CeO_2/\alpha\text{-}Al_2O_3(0001)$ sample after several different pre-treatments. The AFM image obtained after ceria deposition and oxidation in air at 773 K shows that the surface is covered with round features approximately 40 nm in diameter. These features were absent in images obtained form the clean $\alpha\text{-}Al_2O_3(0001)$ substrate indicating that they are due to the ceria layer. The observation that the ceria film does not grow in a layer-by-layer fashion is consistent with the fact that vapor-deposited ceria films $\alpha\text{-}Al_2O_3(0001)$ are polycrystalline [9,28,30].

An AFM image obtained after annealing the $CeO_2/\alpha\text{-}Al_2O_3(0001)$ sample at 1273 K in air for 12 hrs is shown in Figure 5-B. The round, ceria features observed after annealing at lower temperatures have coalesced to form a fewer number of larger features with a similar shape. Relatively large triangular pyramid shaped features have also appeared that have a lateral dimension of ~0.25 μm. As noted above, the XPS results show that annealing the $CeO_2/\alpha\text{-}Al_2O_3(0001)$ sample in air at 1273 K induces the reduction of a significant fraction of the ceria cations from +4 to +3 suggesting the formation of $CeAlO_3$. Cerium aluminate has a cubic perovskite structure. Growth of $CeAlO_3$ particles with the (111) plane parallel to the (0001) surface of the $\alpha\text{-}Al_2O_3(0001)$ would be expected to produce triangular pyramid shaped features (i.e. the corners of a cube coming out from the surface). Thus, one interpretation of this image is that the round shaped features are composed of either CeO_2 or $CeAl_{1-x}O_{3-x}$ ($x \leq 1$) and the pyramids are composed of $CeAlO_3$.

Heating the $CeO_2/\alpha\text{-}Al_2O_3(0001)$ sample that was previously annealed in air that contained the pyramid shaped features in vacuum to 973 K caused additional changes in the morphology of the ceria film. In addition to the pyramids, long triangular bar-shaped features have emerged. Since the XPS results show that this sample contains primarily Ce^{+3}, these bar-

shaped features are also likely to be composed of $CeAlO_3$. The XPS results also suggest that the round features cannot be composed of CeO_2. While a sub oxide of ceria such as Ce_2O_3 is a possibility this assignment is not consistent with the XPS results in Figure 2 that show that CeO_2 films on α-Al_2O_3(0001) do not undergo reduction upon heating to 973 K in vacuum. While additional study is needed in order to obtain a definitive assignment, the data suggests that the round features in image C are composed of $CeAl_{1-x}O_{3-x}$ ($x \leq 1$).

4. Discussion

The results obtained in this study provide considerable insight into the structure and thermal stability of ceria films supported on both YSZ(100) and α-Al_2O_3(0001). The AFM studies show that vapor deposition of cerium metal followed by oxidation under relatively mild conditions produces a continuous CeO_2 film on YSZ(100). This result is consistent with previous X-ray diffraction [28]and TEM [9] studies that have shown that vapor-deposited CeO_2 forms an epitaxial overlayer on YSZ(100). Epitaxial growth is facilitated by the fact that YSZ and ceria both have cubic fluorite structures and a relatively small lattice mismatch of 5.5 % [28]. In contrast to CeO_2/YSZ(100), vapor-deposited ceria films on α-Al_2O_3(0001) were composed of round ceria islands. This result is also consistent with previous studies that have shown that vapor deposition produces polycrystalline CeO_2 films on α-Al_2O_3(0001) [9].

For both CeO_2/YSZ(100) and CeO_2/α-Al_2O_3(0001) the structure of the ceria layer was found to be influenced by annealing under oxidizing and reducing environments. Annealing a CeO_2/YSZ(100) sample in air at 1273 K caused the ceria film to agglomerate into bar-shaped structures that are aligned with distinct crystallographic directions of the YSZ(100) support. As noted in a previous letter [33], the fact that the ceria film undergoes some structural

modifications upon annealing in air is not particularly surprising. The extent of the structural changes and the temperature range in which they occur, however, is unusual. Given that CeO_2 has a melting temperature of 2875 K one would expect a high degree of structural stability for a ceria film under oxidizing conditions. The AFM results show that this is not the case and that the CeO_2 film on YSZ(100) undergoes agglomeration into oriented bar shaped features upon annealing in air at only 1273 K. Furthermore, this agglomeration is at least partially reversible by annealing in vacuum at temperatures as low as 873 K. These results may have implications for catalytic applications which make use of ceria-zirconia interfaces. For example, in automotive emissions control systems the air-to-fuel ratio in the engine exhaust undergoes transients from the desired stoichiometric value required for complete combustion of residual hydrocarbons and CO into both fuel rich (i.e. reducing) and fuel lean (i.e. oxidizing) conditions. The results of this study suggest that these oscillations in the air-to-fuel ratio may be accompanied by changes in the structure of the ceria/zirconia component of the catalyst.

The AFM results obtained in this study also show that CeO_2 films on α-Al_2O_3(0001) undergo restructuring upon annealing in air at 1273 K resulting in the formation of large ceria clusters and triangular pyramidal and long triangular bar-shaped features. The fact that XPS showed that annealing in air was accompanied by reduction of a significant fraction of the Ce cations from +4 to +3 suggests that reaction of the ceria with the alumina substrate to form $CeAlO_3$ is the driving force for this agglomeration process. This conclusion is consistent with previous studies of the interaction of ceria with high surface area γ-Al_2O_3 [20,21,40]. For example Damyanova et al. [20] and Shyu et al. [21] report that calcining samples consisting of low loadings of CeO_2 (<6 wt.%) on γ-Al_2O_3 in air at 1073 K results in partial reduction of the ceria. This was attributed to a strong interaction between the ceria and the alumina support and

the formation of a cerium aluminate "precursor" which is easily converted to $CeAlO_3$ upon reduction in H_2 at temperatures above 800 K [20,21]. This latter observation is also consistent with the results presented here. The XPS spectrum of the air-annealed $CeO_2/\alpha\text{-}Al_2O_3(0001)$ sample contained both Ce^{+3} and Ce^{+4}, while only Ce^{+3} was observed after annealing this sample in vacuum at 873 K. It is interesting that in spite of the fact that the cerium cations undergo reduction, an oxidizing environment appears to be necessary in order to initiate the formation of $CeAlO_3$ from CeO_2 films supported on alumina. Note that the XPS data in Figure 2 shows that $CeO_2/\alpha\text{-}Al_2O_3(0001)$ samples that have not been previously annealed in air (or oxygen) at temperatures above 450 K are stable upon heating to 1000 K in vacuum.

Finally, this study serves to further demonstrate that interactions between ceria and an oxide support can dramatically influence the reducibility of the ceria. CeO_2 films supported on $\alpha\text{-}Al_2O_3(0001)$ were found to be stable upon heating to 1000 K in vacuum and XP spectra of a sample treated in this manner contained predominantly Ce^{+4}. This is in contrast to epitaxial CeO_2 films on YSZ(100) which were found to be reduced upon heating to temperatures in excess of 825 K in vacuum [29,33]. In the present study, oriented CeO_2 particles supported on YSZ(100), which were formed by annealing a CeO_2/YSZ(100) sample in air at 1273 K, were also found to undergo reduction to Ce_2O_3 upon heating to only 873 K in vacuum.

The observation of the reduction of CeO_2 supported on YSZ(100) at relatively low temperatures is quite surprising in light of the fact that bulk thermodynamics predicts that CeO_2 should be stable under the conditions used in our experiments. For example, based on the equilibrium constant for the reduction of CeO_2 to $CeO_{1.83}$ [41-43] the onset of reduction of CeO_2 at 825 K should occur at an oxygen partial pressure of $\sim 10^{-28}$ atm. This is well below the P_{O_2} in our UHV system, which was estimated to be $\sim 10^{-15}$ atm via mass spectrometry. For this P_{O_2}

equilibrium calculations predict that the onset of reduction of CeO_2 should occur near 1200 K. This prediction is consistent with the results obtained here for CeO_2/α-Al_2O_3(0001) which remained fully oxidized upon heating to 1000 K in UHV and with a previous study that showed that the onset of O_2 desorption from a CeO_2(111) single crystal in UHV indeed occurs near 1200 K [44].

5. Conclusions

The results of this study provide insight into the effect of temperature and gas environments on the structure of ceria films supported on YSZ(100) and α-Al_2O_3(0001). Vapor-deposited ceria films on YSZ(100) form epitaxial overlayers that are stable in oxidizing environments at temperatures up to 825 K. At higher temperatures, under oxidizing conditions YSZ(100)-supported ceria undergoes agglomeration forming oriented, bar shaped structures. Subsequent annealing in vacuum at 973 K causes partial redistribution of the ceria film over the YSZ(100) surface. Polycrystalline ceria films on α-Al_2O_3(0001) were also found to agglomerate upon annealing in air at 973 K. Annealing at higher temperatures (1273 K) in air caused a reaction between the ceria and the alumina substrate to produce $CeAlO_3$.

Significant differences in the reducibility of ceria films on YSZ(100) and α-Al_2O_3(0001) were also observed. α-Al_2O_3(0001) supported CeO_2 remained fully oxidized upon heating to 1000 K in vacuum, while YSZ(100) supported CeO_2 was reduced to Ce_2O_3 upon heating to only 825 K in vacuum.

Acknowledgements

The authors are grateful to the U.S. Office of Naval Research for providing funding for this work.

References

[1] J. Kaspar, P. Fornasiero, and M. Graziani, Catal. Today 50 (1999) 285.

[2] A. Trovarelli, Catal. Rev. 38 (1996) 439.

[3] A. Trovarelli (ed), Catalysis by Ceria and Related Materials, Imperial College Press, London, 2002.

[4] H.S. Gandhi, M. Shelef, Stud. Surf. Sci. Catal. 30 (1987) 199.

[5] R.K. Herz, J.A. Sell, J. Catal. 94 (1985) 199.

[6] R.W. McCabe, J.M. Kisenyi, Chem. Ind. 15 (1995) 605.

[7] K. Otsuka, M. Hatano, A. Morikana, J. Catal 79 (1983) 493.

[8] M. Shelef, G.W. Graham, Catal. Rev. 36 (1994) 433.

[9] E.S. Putna,T. Bunluesin, X.L. Fan, R.J. Gorte, J.M. Vohs, R.E. Lakis, T. Egami, Catal. Today 50 (1999) 343.

[10] P. Fornasiero, R.D. Monte, G.R. Rao, J. Kaspar, S. Meriani, A. Trovarelli, M. Graziani, J. Catal. 151 (1995) 168.

[11] M. Haneda, K. Miki, N. Katusa, A. Ueno, S. Matsuura, M. Sato, Nihon Kagatu Kaishi 8 (1990) 820.

[12] T. Ohatu, Rare Earths 17 (1990) 37.

[13] N.P. Brandon, S. Skinner, and B.C.H. Steele, Annu. Rev. Mater. Res. 33 (2003) 183.

[14] M. Mogensen, in A. Trovarelli (ed.), Catalysis by Ceria and Related Materials, Imperial College Press, London, 2002, p. 453.

[15] A. Atkinson, S. Barnett, R.J. Gorte, J.T.S. Irvine, A.J. McEvoy, M. Mogensen, S.C. Singhal, J. Vohs, Nature Materials 3 (2004) 17.

[16] S. Park, J.M. Vohs, R.J. Gorte, Nature 404 (2000) 265.

[17] R.J. Gorte, J.M. Vohs, J. Catal. 216 (2003) 477.

[18] O. A. Marina, M. Mogensen, Appl. Catal. A 189 (1999) 117.

[19] A. Piras, A. Trovarelli, G. Dolcetti, Appl. Catal. B 28 (2000) L77.

[20] S. Damyanova, C.A. Perez, M. Schmal, J.M.C. Bueno, Appl. Catal.s A 234 (2002) 271.

[21] J.Z. Shyu, W.H. Weber, H.S. Gandhi, J Phys Chem. 92 (1988) 4964.

[22] J.Z. Shyu, K. Otto, W.L.H. Watkins, G.W. Graham, R.K. Belitz, H.S. Gandhi, J. Catal. 114 (1988) 23.

[23] J.S. Church, N.W. Cant, D.L. Trimm, Appl Catal. A 101 (1993) 105.

[24] Y.J. Kim, S. Thevuthasan, V. Shutthananadan, C.L. Perkins, D.E. McCready, G.S. Herman, Y. Gao, T.T. Tran, S.A. Chambers, C.H.F. Peden, J Elec. Spectrosc. Relat. Phenom. 126 (2002) 177.

[25] C.M. Wang, S. Thevuthasan, C.H.F. Peden, J. Am. Ceram. Soc. 86 (2003) 363.

[26] R.M. Ferrizz, G.S. Wong, T. Egami, J.M. Vohs, Langmuir 17 (2001) 2464.

[27] R.M. Ferrizz, T. Egami, J.M. Vohs, Catal Lett 61 (1999) 33.

[28] W. Dmowski, T. Egami, R. Gorte, J. Vohs, Physica B 221 (1996) 420.

[29] R.M. Ferrizz, T. Egami, G.S. Wong, J.M. Vohs, Surf. Sci. 476 (2001) 9.

[30] W. Dmowski, E. Mamontov, T. Egami, S. Putna, R. Gorte, Physica B 248 (1998) 95.

[31] S.A. Maicaneanu, D.C. Sayle, G.W. Watson, J. Phys. Chem. B 105 (2001) 12481.

[32] D.C. Sayle, S.A. Maicaneaunu, G.W. Watson, J. Am. Chem. Soc. 124 (2002) 11429.

[33] O. Costa-Nunes, R.J. Gorte, J.M Vohs, J. Mater. Chem. DOI:10.1039/b416670a (2005).

[34] D.R. Mullins, S.H. Overbury, D.R. Huntley, Surf. Sci. 409 (1998) 307.

[35] A. Fujimori, Phys. Rev. B 28 (1983) 2281.

[36] A. Fujimori, Phys. Rev. B 27 (1983) 3992.

[37] A. Fujimori, Phys. Rev. B 28 (1983) 4489.

[38] P. Burroughs, A. Hamnett, A.F. Orchard, and G. Thornton, J. Chem. Soc. Dalton Trans. 17 (1976) 1686.

[39] A. Kotani, T. Jo, J.C. Parlebas, Adv. Phys. 37 (1988) 37.

[40] S. Humbert, A. Colin, L. Monceaux, F. Oudet, P. Courtine, Stud. Surf. Sci. Catal. 96 (1995) 829.

[41] R.M. Ferrizz, R.J. Gorte, J.M. Vohs, Appl Catal B 43 (2003) 273.

[42] D.A.R. Kay, W.G. Wilson, V. Jalan, J Alloy Compd. 193 (1993) 11.

[43] R.K. Dwivedi, D.A.R. Kay, J. Less-Common Met. 102 (1984) 1.

[44] E.S. Putna, J.M. Vohs, R.J. Gorte, J Phys Chem. 100 (1996) 17862.

Pre-treatment	Ce(3d)/Zr(3d)
Annealed in air at 773 K	20.6
Annealed in air at 1273 K	2.3
Annealed in vacuum at 873 K	2.2
Annealed in vacuum at 973 K	4.1

Table 1.
Ratio of the areas of the Ce(3d) and Zr(3d) peaks for the CeO_2/YSZ(100) sample as a function of pretreatment conditions.

Pre-treatment	Ce(3d)/Al(2p)
Annealed in air at 773 K	97
Annealed in air at 1273 K	7
Annealed in vacuum at 873 K	12
Annealed in vacuum at 973 K	16

Table 2.
Ratio of the areas of the Ce(3d) and Al(2p) peaks for the $CeO_2/\alpha\text{-}Al_2O_3(0001)$ sample as a function of pretreatment conditions.

Figure Captions

Figure 1. XP spectra of the Ce(3d) region of (A) CeO_2/YSZ(100) sample after heating in vacuum to 450 K, (B) after annealing sample (A) in vacuum at 750 K, (C) after annealing sample (B) in vacuum at 825 K, (D) after annealing sample (C) in vacuum at 900 K.

Figure 2. XP spectra of the Ce(3d) region of (A) CeO_2/Al_2O_3(0001) sample after heating in vacuum at 550 K, (B) after annealing sample (A) in vacuum at 750 K, (C) after annealing sample (B) in vacuum at 825 K, (D) after annealing sample (C) in vacuum at 900 K, (E) after annealing sample (D) in vacuum at 1000 K.

Figure 3. XP spectra of the Ce(3d) region of (A) CeO_2/Al_2O_3(0001) sample after oxidation in air at 773 K for 12 hrs, (B) after annealing sample (A) in air at 973 K for 12 hrs, (C) after annealing sample (A) in air at 1273 K for 12 hrs, (D) after heating sample (C) in vacuum at 873 K for 2 hrs.

Figure 4. AFM images CeO_2/YSZ(100) sample (A) after deposition and calcination in air at 773 K,(B) after annealing sample (A) in air at 1273 K, and (C) after annealing sample (B) in vacuum at 973 K.

Figure 5. AFM images of CeO_2/Al_2O_3(0001) sample (A) after deposition and calcination in air at 773 K, (B) after annealing sample (A) in air at 1273 K, and (C) after annealing sample (B) in vacuum at 973 K.

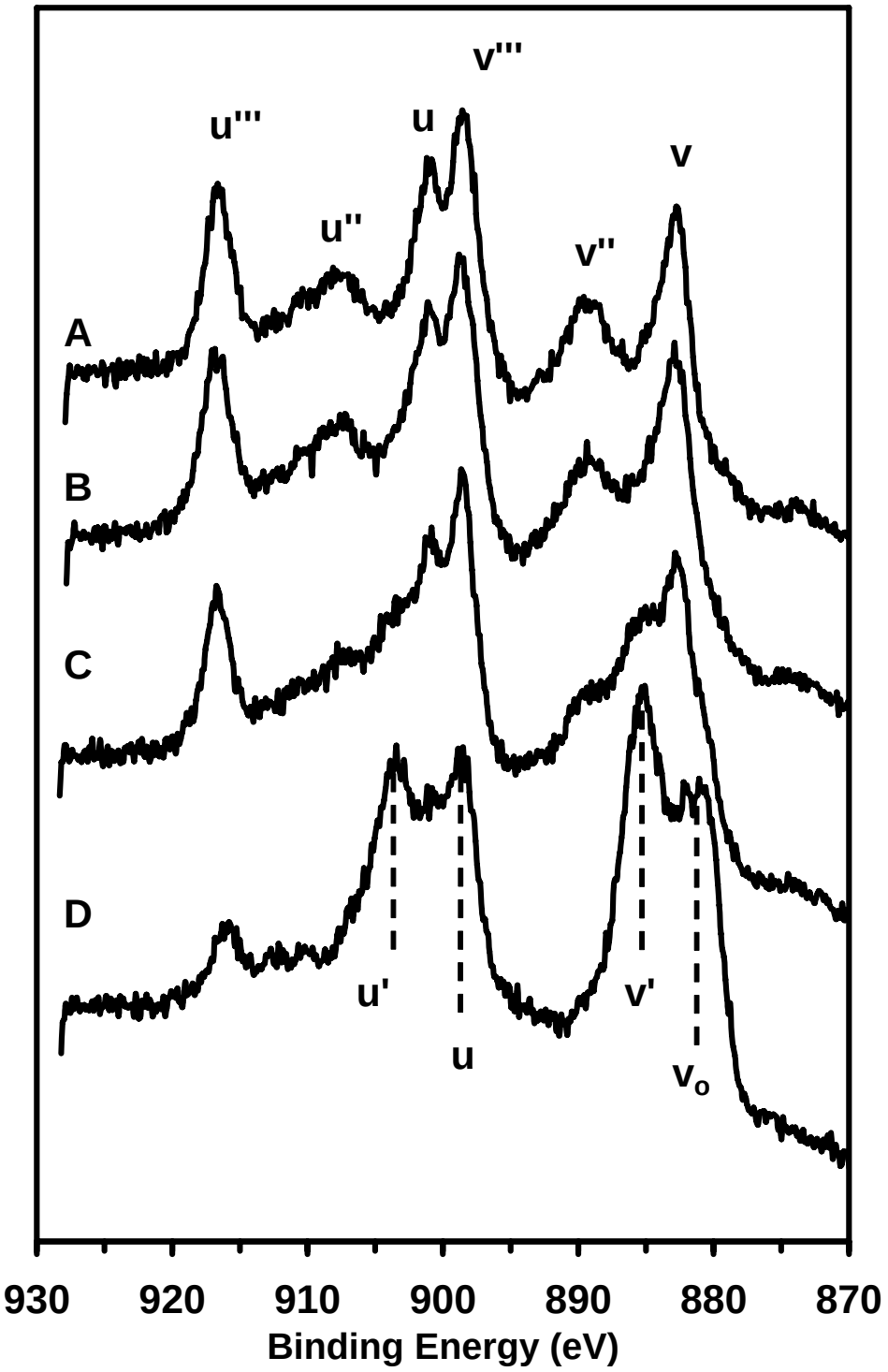
v'''
u'''
u
v
u''
v''
A
B
C
D
u'
u
v'
v_o
930
920
910
900
890
880
870
Binding Energy (eV)

Figure 1

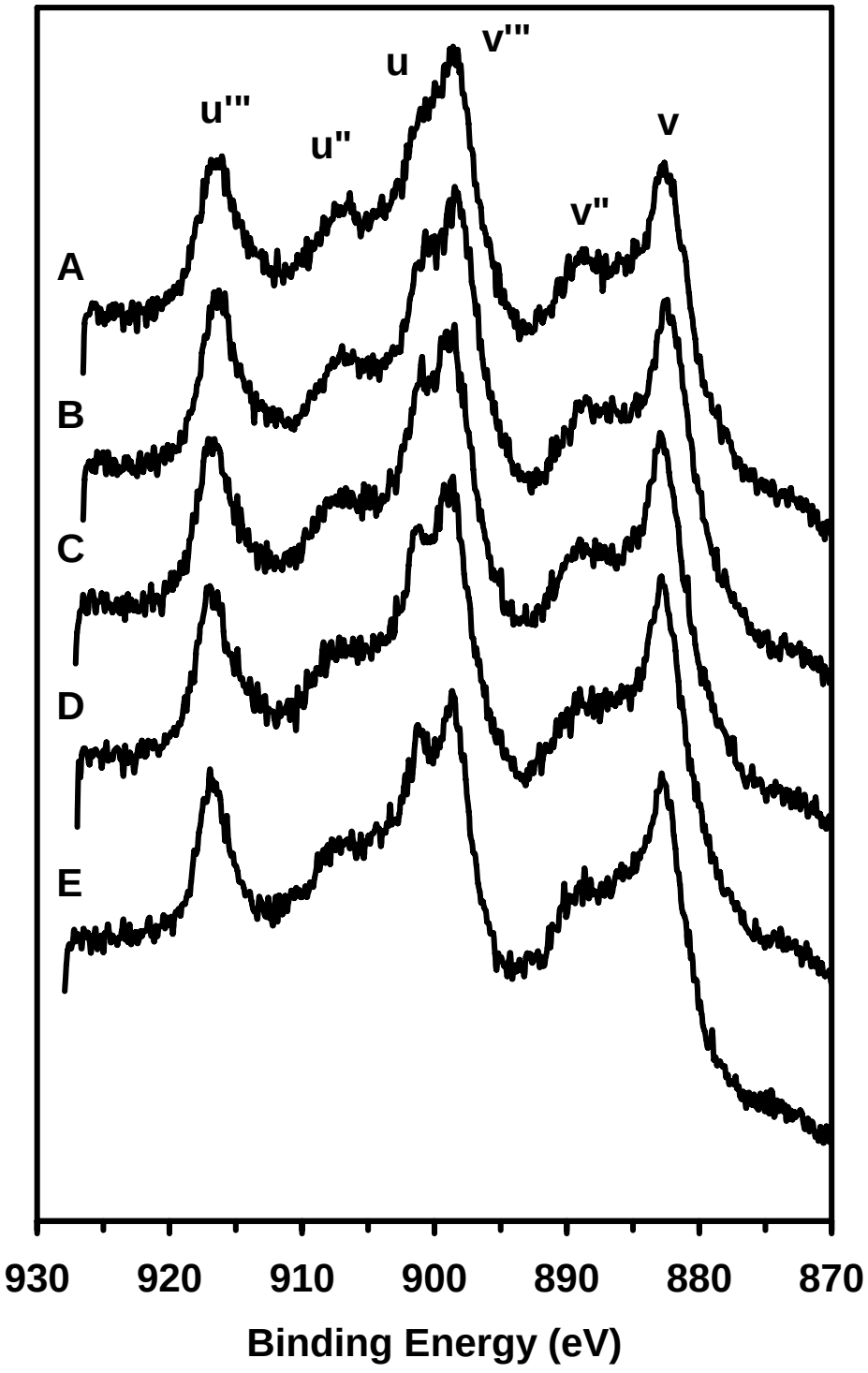

Figure 2

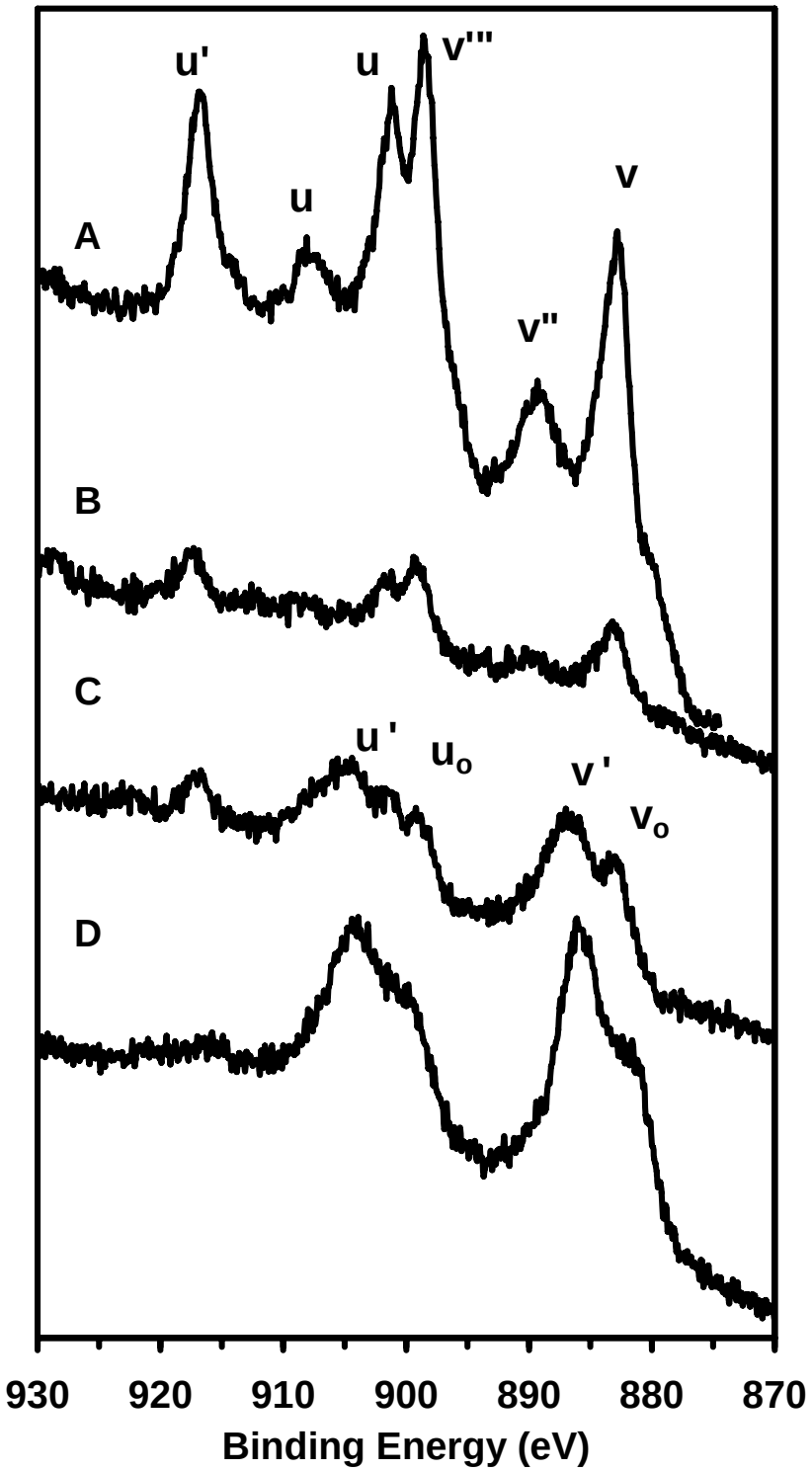
u'
u
v'''
u
v
A
v''
B
C
u '
u_o
v '
v_o
D
930
920
910
900
890
880
870
Binding Energy (eV)

Figure 3

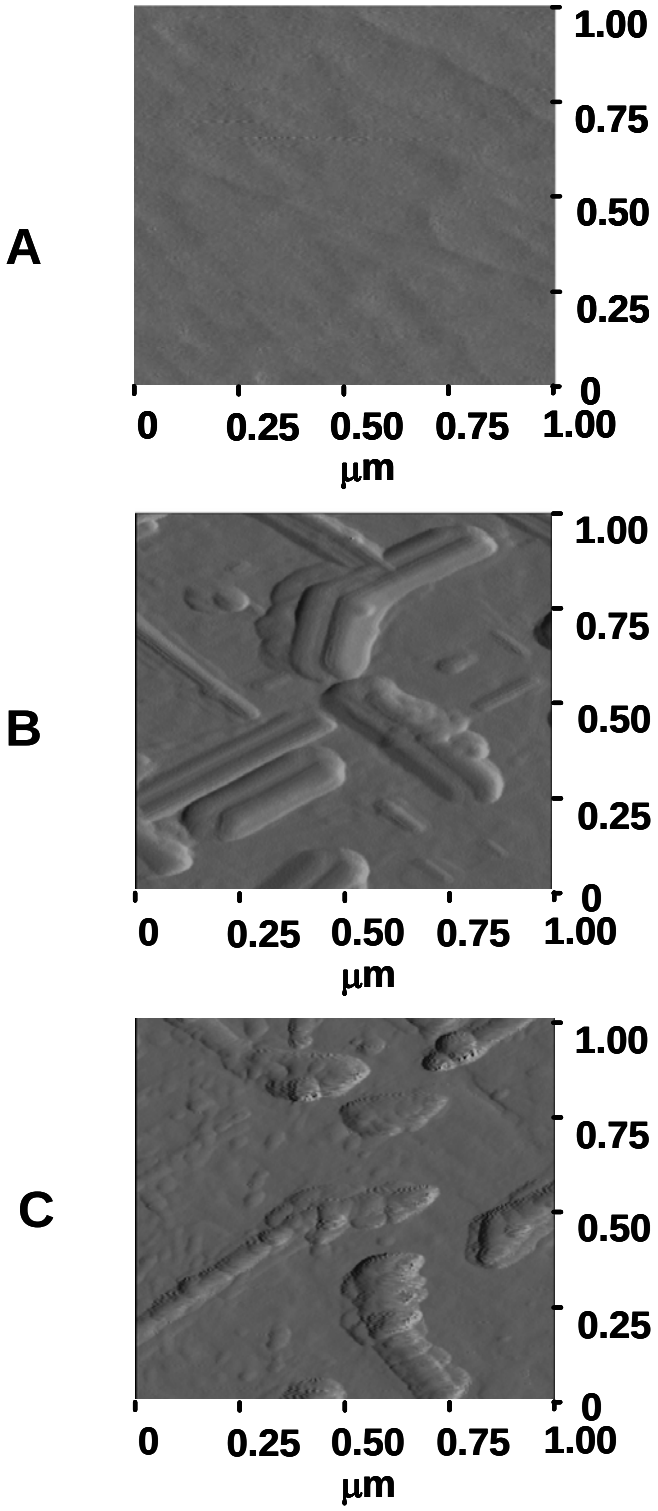

Figure 4

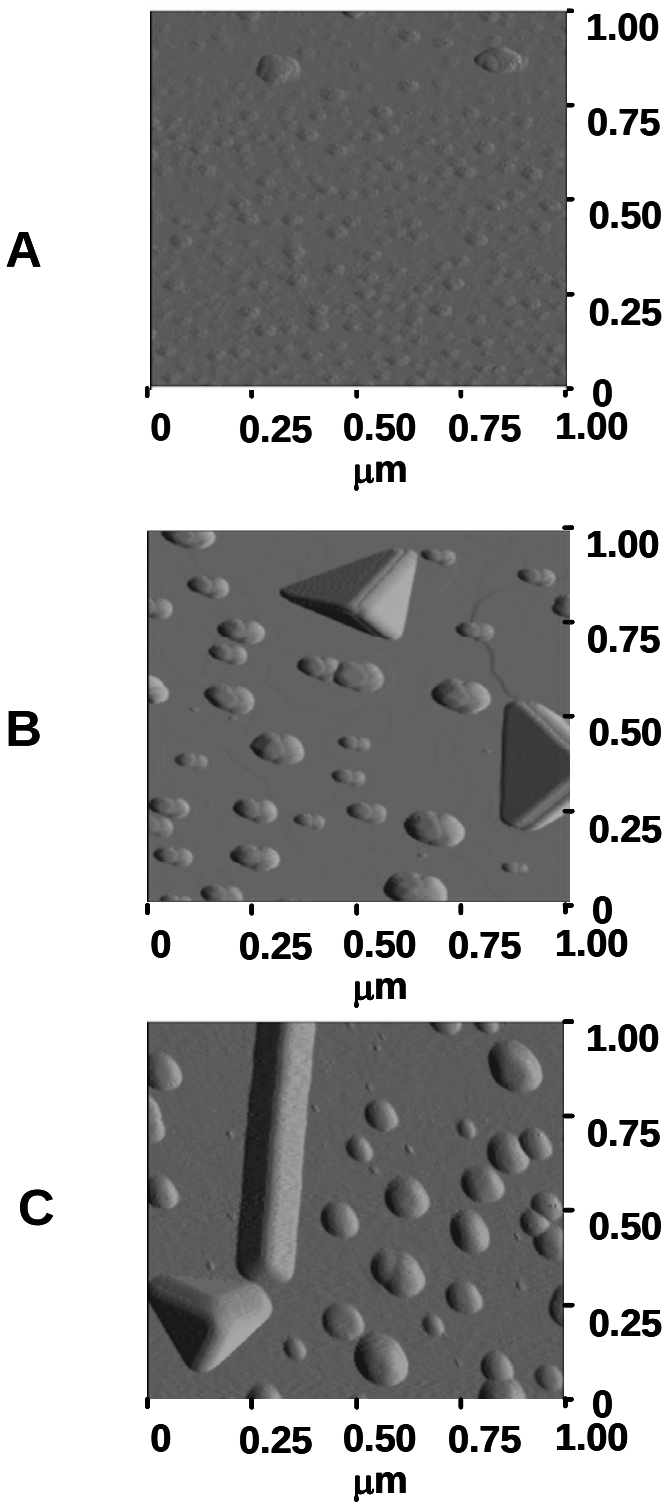

Figure 5